Grenze International Journal of Engineering and Technology, June Issue

CFD Investigation of Pulsatile Blood Flow in Axisymmetric Stenosed Porous Arteries with Velocity Slip Effects

Priyanga R[1] and Girija Bai H[2]
[1]Research Scholar, Mathematics Department, Sathyabama Institute of Science and Technology, Chennai, India.
Email: priyangaravi6@gmail.com
[2]Assistant Professor, Mathematics Department, Sathyabama Institute of Science and Technology, Chennai, India
Email: girijanameprakash@gmail.com

***Abstract*— Blood flow plays a critical role in the development of atherosclerosis, where clots and plaques can restrict arterial blood transport. This study presents a computational investigation of unsteady, incompressible, electrically conducting, and viscous blood flow through multiple stenosed porous channels, incorporating magnetohydrodynamic (MHD) effects and slip velocity at permeable walls under time-dependent infusion or suction conditions. The governing equations are solved analytically using a perturbation method, yielding expressions for axial velocity (u_x), volumetric flow rate (Q_v), and wall shear stress (WSS, τ_w). Numerical simulations based on the Finite Volume Method illustrate the influence of key physical parameters on u_x, Q_v and τ_w providing insights into hemodynamic behavior and potential implications for the onset and progression of arterial diseases. To validate the analytical predictions, computational fluid dynamics (CFD) simulations were performed using ANSYS Fluent based on the finite volume method. The numerical results, including axial velocity, pressure distribution, and wall shear stress contours, showed good agreement with the analytical findings. The combined analytical and CFD investigation provides a comprehensive understanding of the hemodynamic behavior in multiple-stenosed porous arteries and highlights the influence of stenosis severity on blood flow characteristics.**

***Index Terms*— MHD, Multiple stenosis, Pulsatile blood flow, porous channel and Slip velocity.**

I. INTRODUCTION

Fluid dynamics studies how pressures, including external ones, influence fluid motion. Blood is a circulatory fluid transported by the heart throughout the body. Recent studies indicate that coronary artery disease (CAD) is a leading cause of death in India and a major global cause of disability, with mortality in Indians expected to rise sharply, surpassing high-income countries. Understanding blood flow is therefore crucial for diagnosing arterial diseases and developing preventive strategies. Computational models have been widely used to study stenosed arteries. Ali A. et al. [1] investigated MHD pulsatile micropolar flow in channels with symmetric constrictions. Azmi W. et al. [2] gives the mathematical modelling of MHD blood flow with gold nanoparticles in slip small arteries.
Chen X. et al. [3] studied the effects of stenosis rate and Reynolds number on local flow and plaque formation.

Grenze ID: 01.GIJET.12.2.130_26

Farooq J. and Hussain M. [7] gives analysis of MHD slip blood flow through a constricted artery filled with a porous medium of variable permeability: Applications in Biomedical Engineering.
Shaikh F. et al. [8] compared numerical simulations of blood flow through stenosed segments. Satwai N. and Prasad K. M. [11] Modelling of MHD micropolar nano fluid flow in an inclined porous stenosed artery with dilatation. Thirunanasambantham et.al. [12] Computational Analysis of Hybrid GPL Blood Nanofluid Flow Through a Stenosed Artery Under MHD Effects. Ganesh S. et al. [9] analyzed MHD unsteady flow in narrow channels. Girija Bai H. [19], [20] explored pressure variations and blood flow in stenosed arteries. Hussain A. et al. [18] modeled blood flow through stenosed channels. Umar M. [21] gives the numerical simulations of blood flow in a stenosed artery using a multi-criteria decision-making algorithm.
This work investigates unsteady pulsatile blood flow in a multiple-stenosed porous channel with time-dependent boundary velocity (injection/suction) and electromagnetic effects. The governing equations are solved analytically and parametric solutions are obtained via the finite volume method (FVM). Key parameters $(K_p, \delta, M, \lambda, R)$ affect velocity, wall shear stress, pressure drop, stent performance and disease progression, emphasizing their importance for personalized treatment and optimized outcomes.

II. Mathematical Formulation

Figure 1 shows the computational model of a multiple-stenosed porous channel. A Cartesian coordinate system (x, y) is used, where the x-axis is aligned with the channel centerline and the y-axis is perpendicular to it. Blood is assumed to be an unsteady, viscous, incompressible, electrically conducting Newtonian fluid subjected to a uniform transverse magnetic field of strength M_0. Owing to the low magnetic Reynolds number, induced electromagnetic effects are neglected. The channel is considered porous and permeable, allowing limited fluid exchange through its walls.

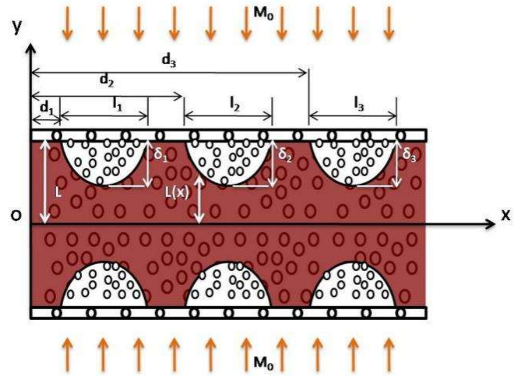

Figure 1. The flow configuration's geometry with multiple stenosis

The 2D equations that govern continuity and momentum (in both x and y directions) have been provided as dimensional notation based on the previous assumptions as follows:

$$\frac{\partial u_x}{\partial x} + \frac{\partial v_y}{\partial y} = 0 \qquad (1)$$

$$\frac{\partial u_x}{\partial t} + u_x \frac{\partial u_x}{\partial x} + v_y \frac{\partial u_x}{\partial y} = -\frac{1}{\rho}\frac{\partial p}{\partial x} + \nu\left(\frac{\partial^2 u_x}{\partial x^2} + \frac{\partial^2 u_x}{\partial y^2}\right) - \left(\frac{\nu}{k}\right) u_x - \frac{\sigma_e M_0^2 u_x}{\rho} \qquad (2)$$

$$\frac{\partial v_y}{\partial t} + u_x \frac{\partial v_y}{\partial x} + v_y \frac{\partial v_y}{\partial y} = -\frac{1}{\rho}\frac{\partial p}{\partial y} + \nu\left(\frac{\partial^2 v_y}{\partial x^2} + \frac{\partial^2 v_y}{\partial y^2}\right) - \left(\frac{\nu}{k}\right) v_y \qquad (3)$$

where u_x and v_y → velocity components on x and y $axis, t$ → $time$, ν → kinematic viscosity, p → pressure of blood, ρ →blood density, σ_e →electrical conductivity and k →porous media permeability.
As stated in Makinde and Chinyoka [10], the flow flux is defined to account for the fluid absorbing in the walls

$$\int_{-L}^{L} u_x \, dy = U_x \, f\left(\frac{x}{2L}\right)\left(1 + \epsilon\, e^{i\,\omega\, t}\right), \qquad (4)$$

Let U_x be the initial axial velocity at x=0 and f(x/2L) a flux function describing fluid absorption through the porous wall. The normal velocity through the porous boundary is time-dependent:

$$V = V_u(1 + \epsilon e^{i\omega t}), \qquad (5)$$

where $V_u > 0$ for infusion, $V_u < 0$ for suction, and $\epsilon < 1$ is a small oscillatory amplitude. With homogeneous porous media, $v_y = V$ is independent of x and y, reducing $\partial u_x/\partial x = 0$ and making $u_x = u_x(y,t)$. The pressure gradient along y simplifies to

$$-\frac{\partial p}{\partial y} = \rho V_u(i\omega\epsilon e^{i\omega t}) + \frac{\nu V_u}{k}(1 + \epsilon e^{i\omega t}) \qquad (6)$$

and the axial momentum equation becomes

$$\frac{\partial u_x}{\partial t} + V_u(1 + \epsilon e^{i\omega t})\frac{\partial u_x}{\partial y} = -\frac{1}{\rho}\frac{\partial p}{\partial x} + \nu\frac{\partial^2 u_x}{\partial y^2} - \frac{\nu}{k}u_x - \frac{\sigma_e M_0^2}{\rho}u_x. \qquad (7)$$

The unsteady pressure gradient is assumed as Eldesoky [5]:

$$-\frac{\partial p}{\partial x} = P_g + \epsilon P_a\cos(\omega t), \qquad (8)$$

where P_g and P_a are the steady and pulsatile components, respectively.
The axisymmetric multiple stenosis geometry follows Dawood [4] Eldesoky [6], Prasad et al. [11], Mishra et al. [13], Misra et al. [16] and Shit and Roy [17].
Its dimensionless height is

$$L(x) = \begin{cases} L_0\left[1 - \frac{\delta_1+\delta_2+\delta_3}{2}\left(1 + \cos\frac{2\pi(x-d_c)}{l_c}\right)\right], & d_c \le x \le d_c + l_c, \\ L_0, & \text{otherwise}, \end{cases} \qquad (9)$$

where $d_c = d_1 + d_2 + d_3$, $l_c = l_1 + l_2 + l_3$, δ_i are stenosis heights, $L_0 = 1 - [\cos(2\pi t) - 1]\epsilon e^{-2\pi\epsilon t}$ and $y \in [0, L(x)]$ due to symmetry.
The Beavers–Joseph–Saffman slip condition is applied at the porous wall Beavers [1], Saffman [15] and Bhatt [2]:

$$\begin{aligned} \frac{\partial u_x}{\partial y} &= 0, & y &= 0, \\ u_x &= K_p\frac{\partial u_x}{\partial y}, & y &= L(x), \end{aligned} \qquad (10)$$

where $K_p = \beta/L$ is the slip parameter.
Introducing dimensionless quantities:

$$u_x \to \bar{u}_x = \frac{u_x}{V_u}, \quad x \to \bar{x} = \frac{x}{L}, \quad y \to \bar{y} = \frac{y}{L}, \quad t \to \bar{t} = \frac{\omega t}{2\pi},$$
$$M = \frac{\sigma_e M_0^2 L}{\rho V_u}, \quad W_0 = L\sqrt{\frac{\rho\omega}{\mu}}, \quad R = \frac{LV_u}{\nu}, \quad \lambda = \frac{kV_u}{\nu L}.$$

Applying these, the dimensionless axial momentum equation becomes:

$$\frac{W_0^2}{2\pi R}\frac{\partial u_x}{\partial t} + (1 + \epsilon e^{2\pi}\ )\frac{\partial u_x}{\partial y} = -\frac{\partial p}{\partial x} + \frac{1}{R}\frac{\partial^2 u_x}{\partial y^2} - \left(M + \frac{1}{\lambda}\right)u_x. \qquad (11)$$

III. Solution to the Problem

The axial velocity is assumed in the form

$$u_x(y,t) = u_0(y) + \epsilon u_1(y)e^{2\pi i t}, \qquad (12)$$

where ϵ is the small oscillation amplitude, and u_0, u_1 denote steady and transient components, respectively. Substituting (12) into the governing equations and collecting the coefficients of ϵ^0 and ϵ^1 yields the following.
Steady state (ϵ^0):

$$\frac{1}{R}\frac{d^2u_0}{dy^2} - \frac{du_0}{dy} - \left(M + \frac{1}{\lambda}\right)u_0 = -P_g \qquad (13)$$

with

$$\frac{du_0}{dy} = 0,\ y = 0, \qquad u_0 = K_p \frac{du_0}{dy},\ y = L(x). \qquad (14)$$

The general solution is

$$u_0 = A_1 e^{m_1 y} + A_2 e^{m_2 y} + \frac{P_g}{R\left(M + \frac{1}{\lambda}\right)}, \qquad (15)$$

where,

$$m_{1,2} = 0.5\left[R \pm \sqrt{R^2 + 4R\left(M + \frac{1}{\lambda}\right)}\right], \qquad A_1 = \frac{m_2\left(\frac{P_g}{R\left(M + \frac{1}{\lambda}\right)}\right)}{m_1 m_2 K_p\left(e^{m_1 L(x)} - e^{m_2 L(x)}\right) + m_1 e^{m_2 L(x)} - m_2 e^{m_1 L(x)}},$$

$$A_2 = -\frac{m_1\left(\frac{P_g}{R\left(M + \frac{1}{\lambda}\right)}\right)}{m_1 m_2 K_p\left(e^{m_1 L(x)} - e^{m_2 L(x)}\right) + m_1 e^{m_2 L(x)} - m_2 e^{m_1 L(x)}}.$$

Transient state (ϵ^1):

$$\frac{1}{R}\frac{d^2 u_1}{dy^2} - \left(1 + \epsilon e^{2\pi i t}\right)\frac{du_1}{dy} - \left(M + \frac{1}{\lambda} + \frac{iW_0^2}{R}\right)u_1 = \frac{du_0}{dy} - P_a \cos(2\pi t)\, e^{-2\pi i t}, \qquad (16)$$

subject to

$$\frac{du_1}{dy} = 0,\ y = 0, \qquad u_1 = K_p \frac{du_1}{dy},\ y = L(x). \qquad (17)$$

The solution is

$$u_1 = A_3 e^{m_3 y} + A_4 e^{m_4 y} + A_5 e^{m_1 y} + A_6 e^{m_2 y} + A_7, \qquad (18)$$

where,

$$m_{3,4} = 0.5\left[(\bar{R}) \pm \sqrt{(\bar{R})^2 + 4R\left(M + \frac{1}{\lambda} + \frac{iW_0^2}{R}\right)}\right],\ \bar{R} = R\left(1 + \epsilon e^{2\pi i t}\right) \approx R,$$

$$A_3 = \frac{A_{31} + A_{32} + A_7 m_4}{m_3 e^{m_4 L(x)} - m_4 e^{m_3 L(x)} + m_3 m_4 K_p\left(e^{m_3 L(x)} - e^{m_4 L(x)}\right)},\ A_4 = -\frac{m_1 A_5 + m_2 A_6 + m_3 A_3}{m_4},$$

$$A_5 = \frac{R m_1 A_1}{m_1^2 - m_1 R - R\left(M + \frac{1}{\lambda} + \frac{iW_0^2}{R}\right)},\ A_6 = \frac{R m_2 A_2}{m_2^2 - m_2 R - R\left(M + \frac{1}{\lambda} + \frac{iW_0^2}{R}\right)}, A_7 = \frac{P_a \cos(2\pi t)\, e^{-2\pi}}{M + \frac{1}{\lambda} + \frac{iW_0^2}{R}}.$$

Finally, substituting u_0 and u_1 into (12), the complete velocity profile is obtained as

$$u_x(y,t) = A_1 e^{m_1 y} + A_2 e^{m_2 y} + \frac{P_g}{R\left(M + \frac{1}{\lambda}\right)} + \epsilon e^{2\pi i t}\left(A_3 e^{m_3 y} + A_4 e^{m_4 y} + A_5 e^{m_1 y} + A_6 e^{m_2 y} + A_7\right). \quad (19)$$

Volumetric flow rate:

$$Q_v = \sum_{i=1}^{2} A_i \frac{e^{m_i L(x)} - 1}{m_i} + \frac{P_g L(x)}{R\left(M + \frac{1}{\lambda}\right)} + \epsilon e^{2\pi i t} \sum_{i=3}^{6} A_i \frac{e^{m_i L(x)} - 1}{m_i} + \epsilon e^{2\pi i}\left(A_7 L(x)\right). \qquad (20)$$

Wall shear stress (WSS):

$$\tau_w = \sum_{i=1}^{2} A_i\, m_i e^{m_i L(x)} + \epsilon e^{2\pi i t} \sum_{i=3}^{6} A_i\, m_i e^{m_i L(x)}. \qquad (21)$$

Pressure gradient:

$$-\frac{\partial p}{\partial y} = \frac{L\, i\, \omega\, \epsilon e^{i2\pi t}}{V_u} + \frac{1}{\lambda\rho}(1 + \epsilon e^{i2\pi t}). \qquad (21)$$

IV. NUMERICAL RESULTS AND DISCUSSION

This study provides a numerical analysis of u_x, Q_v and τ_w, computed and displayed via the finite volume method (FVM). Figures 2a-4f show dimensionless profiles for varying slip parameter K_p, stenosis depths δ, magnetic parameter M, permeability λ, and Reynolds number R. Standard parameter values were adopted from Makinde and Osalusi [14], Makinde and Chinyoka [10], and Mishra et al. [13].

Using ANSYS Fluent 2025 R2, CFD simulations were performed to investigate blood flow through a porous artery containing three consecutive stenoses. The continuity and momentum equations were solved under laminar flow conditions using the finite volume method.

Figures 2a-2e illustrate axial velocity profiles. Figure 2a shows a parabolic velocity distribution, with velocity decreasing near the walls and further decreasing as K_p increases. Fig. 2b demonstrates that increasing stenosis depth δ reduces axial velocity near the wall and centerline. Fig. 2c indicates that higher magnetic parameter M lowers axial velocity, a principle used clinically to slow blood flow during surgery. Fig. 2d shows that increased permeability λ enhances axial velocity by reducing flow resistance. Fig. 2e illustrates that increasing R decreases axial velocity in the channel.

Figures 3a-3e present volumetric flow rate Q_v. Flow is lowest at stenosis throats and highest at stenosis ends. Q_v decreases with increasing K_p, δ, M, and R, but rises with higher λ.

Wall shear stress (WSS) is depicted in Figs. 4a-4e. WSS decreases with increasing Kp and λ (Figs. 4a, 4d) and increases with higher δ, M and R (Figs. 4b, 4c and 4e} shows that the pressure gradient $-\partial p/\partial y$ decreases with increasing permeability λ.

The velocity contours (Figure 5) show that blood accelerates significantly at the stenosis throats due to the reduced flow area, reaching maximum values near the center of the artery. Velocity decreases near the walls because of viscous effects and gradually recovers downstream of each constriction.

The pressure contours (Figure 6) reveal a steady pressure decrease along the artery, with larger pressure drops occurring across the stenosed regions. Higher pressure is observed upstream of the constrictions, while lower pressure exists downstream, indicating increased flow resistance.

The wall shear stress distribution (Figure 7) demonstrates peak shear stress at the stenosis throats, where velocity gradients are highest. In contrast, lower and more uniform shear stress values occur in non-stenosed regions. These results highlight the significant impact of multiple stenoses on blood flow dynamics and arterial wall loading.

A. Validation of Analytical Predictions

The CFD simulations reproduce the principal flow characteristics predicted by the analytical formulation. Both approaches indicate accelerated flow through the stenosis throats, a progressive pressure reduction along the artery, and increased wall shear stress in constricted regions. The agreement between the analytical and numerical results demonstrates the reliability of the developed mathematical model for describing pulsatile blood flow in multiple-stenosed porous arteries. Consequently, the CFD analysis serves as an independent verification of the theoretical predictions and provides a detailed visualization of the underlying hemodynamic phenomena.

TABLE I: THE COMPUTED VALUES OF NUMERICAL PARAMETERS ARE DISPLAYED HERE

Kp	δ	M	λ	R	ux1	ux2	ux3	ux4	ux5	ux6	Qv1	Qv2	Qv3	Qv4	Qv5	Qv6	τw1	τw2	τw3	τw4	τw5	τw6
0	0.25	2	0.3	1	0.88	0.86	0.77	0.61	0.36	0	1.18	0.82	0.14	0.07	0.59	1.18	-5.29	-5.11	-3.5	-2.87	-4.88	-5.29
0.1	0.25	2	0.3	1	0.59	0.55	0.44	0.23	0.08	0.23	0.92	0.57	0.01	-0.01	0.35	0.92	-7.35	-7.02	-4.3	-3.39	-6.58	-7.35

1	0.25	2	0.3	1	0.37	0.33	0.19	0.04	-0.04	-0.97	0.69	0.35	-0.06	-0.06	0.15	0.69	-9.13	-8.62	-4.85	-3.72	-7.97	-9.13
0.1	0.1	2	0.3	1	1.24	1.22	1.17	1.06	0.9	0.67	1.17	1.03	0.7	0.64	0.93	1.17	-5.44	-5.39	-5.16	-5.1	-5.34	-5.44
0.1	0.25	2	0.3	1	0.59	0.55	0.44	0.23	0.08	-0.55	1.16	0.8	0.13	0.06	0.57	1.16	-5.44	-5.26	-3.57	-2.91	-5.01	-5.44
0.1	0.5	2	0.3	1	0	-0.05	-0.21	-0.52	-0.99	-1.67	1.15	0.46	-0.05	-0.17	0.11	1.15	-5.44	-4.82	2.09	2.76	-3.42	-5.44
0.1	0.25	0	0.3	1	1.24	1.22	1.17	1.06	0.9	0.67	1.62	1.06	0.14	0.07	0.72	1.62	-6.96	-6.51	-3.85	-3.06	-6	-6.96
0.1	0.25	6	0.3	1	0.59	0.55	0.44	0.23	0.08	-0.55	0.75	0.54	0.11	0.05	0.4	0.75	-4	-3.96	-3.13	-2.67	-3.88	-4
0.1	0.25	9	0.3	1	0	-0.05	-0.21	-0.52	-0.99	-1.67	0.59	0.44	0.1	0.05	0.33	0.59	-3.44	-3.42	-2.88	-2.52	-3.37	-3.44
0.1	0.25	2	0.1	1	0.43	0.4	0.32	0.16	-0.09	-0.5	0.61	0.45	0.1	0.05	0.34	0.61	-3.49	-3.47	-2.91	-2.54	-3.42	-3.49
0.1	0.25	2	0.4	1	0.62	0.58	0.46	0.24	-0.85	-0.56	1.32	0.89	0.13	0.06	0.62	1.32	-5.96	-5.7	-3.68	-2.97	-5.37	-5.96
0.1	0.25	2	0.8	1	0.67	0.63	0.5	0.26	-0.08	-0.58	1.64	1.08	0.14	0.07	0.72	1.64	-7.05	-6.58	-3.86	-3.06	-6.06	-7.05
0.1	0.25	2	0.3	1	0.59	0.55	0.44	0.23	-0.08	-0.55	1.16	0.8	0.13	0.06	0.57	1.16	-5.44	-5.26	-3.57	-2.97	-5.01	-5.44
0.1	0.25	2	0.3	3	0.39	0.37	0.29	0.12	-0.19	-0.79	0.51	0.39	0.1	0.05	0.3	0.51	-3.92	-3.91	-3.41	-2.99	-3.88	-3.92
0.1	0.25	2	0.3	5	0.26	0.24	0.16	-0.04	-0.56	-1.74	0.33	0.26	0.08	0.05	0.2	0.33	-3.5	-3.49	-3.3	-3.04	-3.49	-3.5

Note: Use $K_p = 0.01$ for Q_v and τ_w.

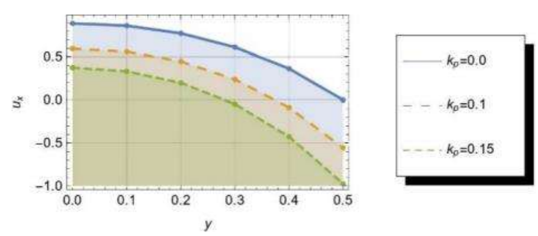

Figure (a) Velocity distribution for increasing the range of the slip parameter K_p

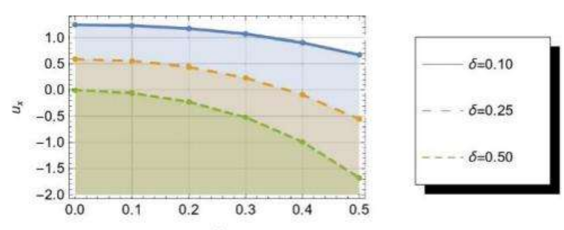

Figure (b) Velocity distribution for increasing the multiple stenose depths $\delta = \delta_1 = \delta_2 = \delta_3$

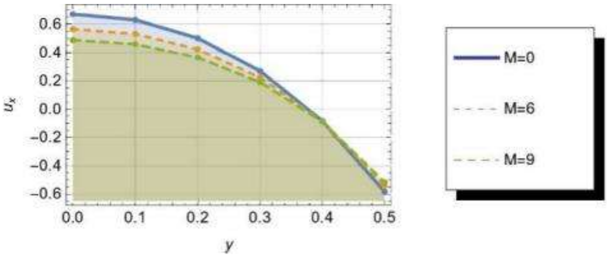

Figure (c) Velocity distribution for increasing the range of the Magnetic parameter M

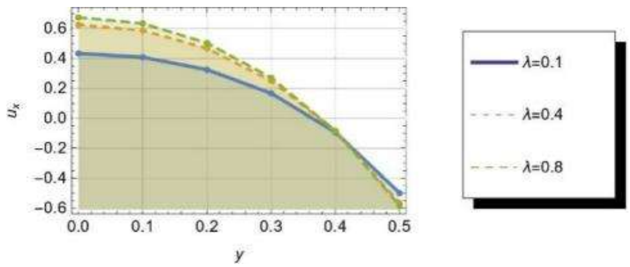

Figure (d) Velocity distribution for increasing the range of the permeability parameter λ.

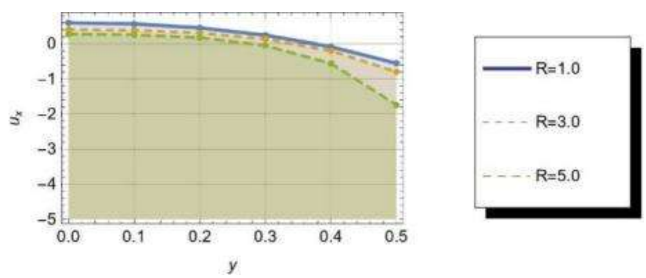

Figure (e) Velocity distribution increasing the range of the Reynolds number R

Figure 2: Velocity distribution under varying parameters: (a) Slip parameter K_p, (b) Stenosis depth δ, (c) Magnetic parameter M, (d) Permeability parameter λ *and* (e) Reynolds number R.

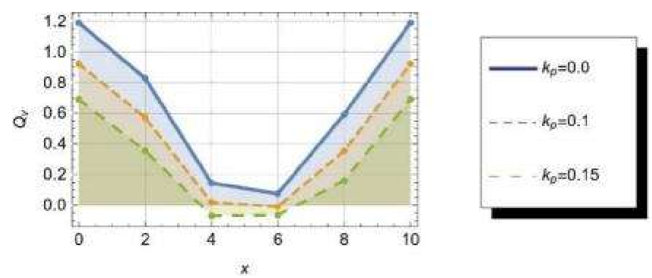

Figure (a) Q_v profile variation as the slip parameter K_p range increases

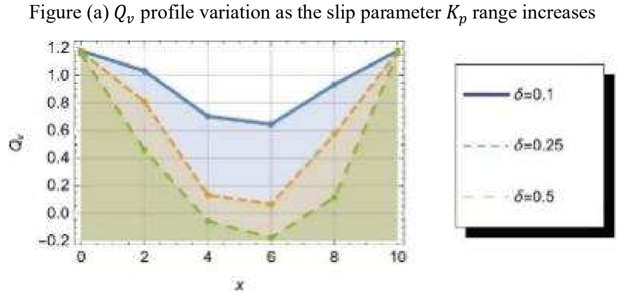

Figure (b) Q_v profile variation as the multiple stenoses depths $\delta = \delta_1 = \delta_2 = \delta_3$ range increases

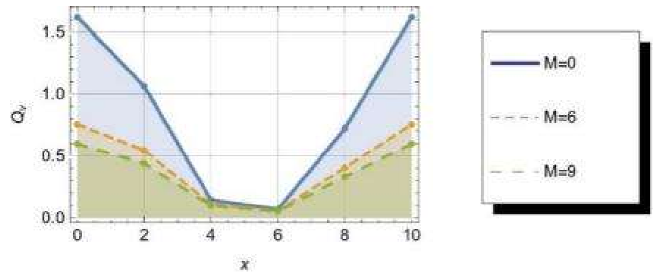

Figure (c) Q_v profile variation as the magnetic parameter M range increases

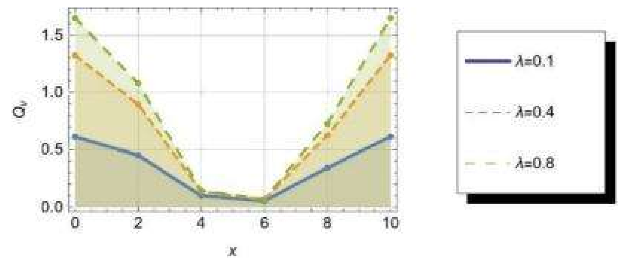

Figure (d) Q_v profile variation as the permeability parameter λ range increases.

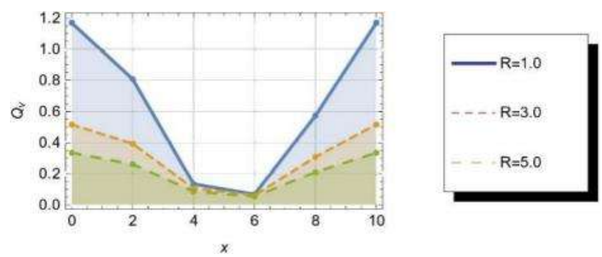

Figure (e) Q_v profile variation as the Reynolds number R range increases

Figure 3: Variation of Q_v profile under different physical parameters: (a) Slip parameter K_p, (b) Stenosis depth δ, (c) Magnetic parameter M, (d) Permeability parameter λ and (e) Reynolds number R

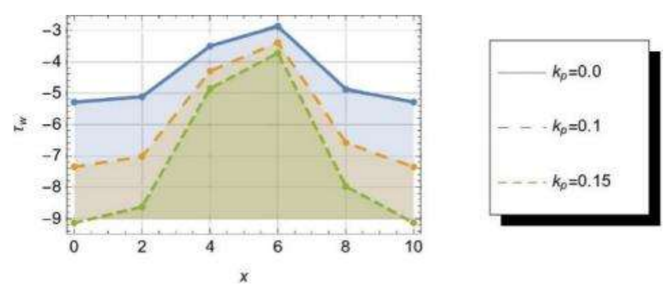

Figure (a) WSS profile variation as the slip parameter K_p range increases

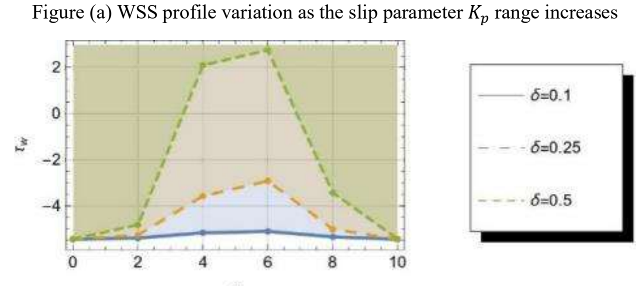

Figure (b) WSS profile variation as the multiple stenoses depths $\delta = \delta_1 = \delta_2 = \delta_3$ range increases

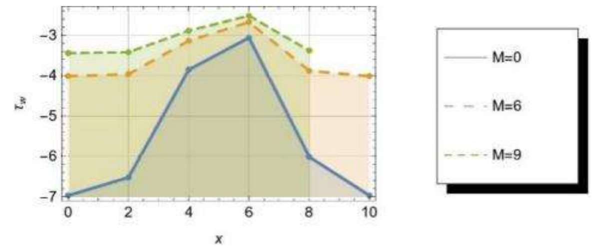

Figure (c) WSS profile variation as the Magnetic parameter M range increases

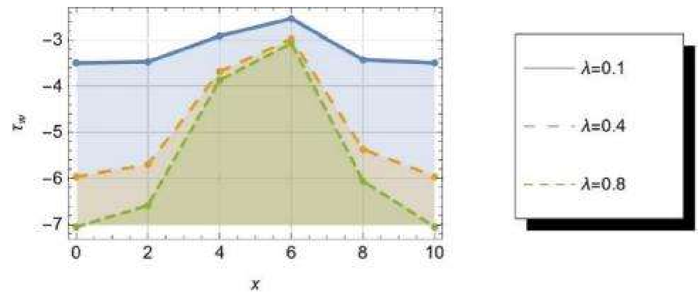

Figure (d) WSS profile variation as the permeability parameter λ range increases

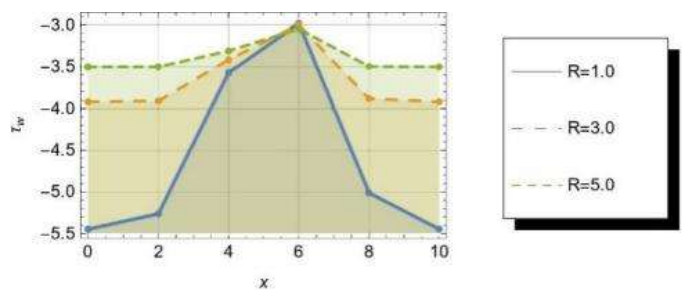

Figure (e) WSS profile as the Reynolds number R range increases

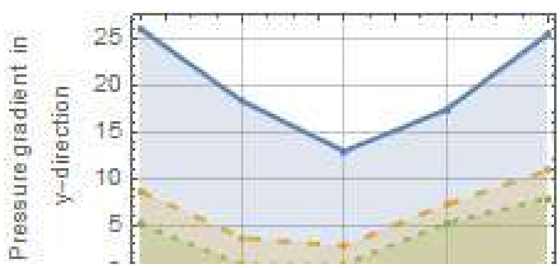

Figure (f) Pressure gradient profile variation $-\frac{\partial p}{\partial y}$ for increasing values of λ when $\epsilon = 0.3$

Figure 4: Profiles of (a–e) Wall Shear Stress (WSS) under varying physical parameters and (f) Pressure gradient variation for permeability parameter λ at $\epsilon = 0.3$.

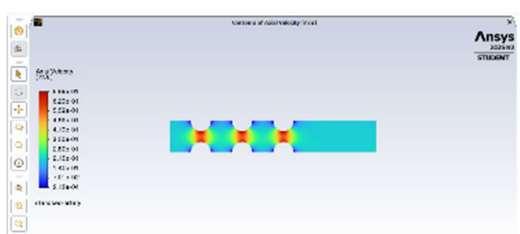

Figure 5: Contour of axial velocity in the triple-stenosed porous artery obtained from ANSYS Fluent.

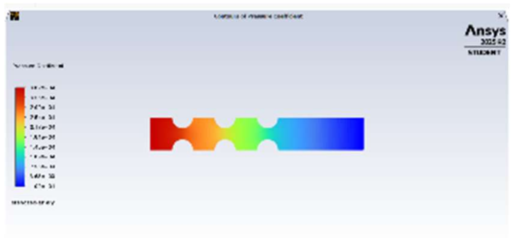

Figure 6: Pressure coefficient distribution along the stenosed artery

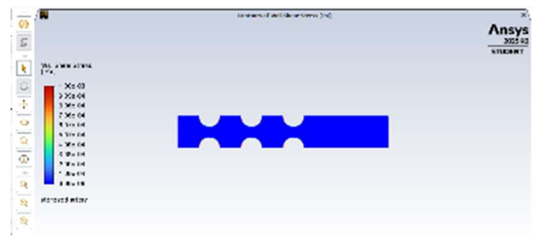

Figure 7: Wall shear stress not Pressure coefficient

B. Validation of Analytical Predictions

The CFD simulations reproduce the principal flow characteristics predicted by the analytical formulation. Both approaches indicate accelerated flow through the stenosis throats, a progressive pressure reduction along the artery, and increased wall shear stress in constricted regions. The agreement between the analytical and numerical results demonstrates the reliability of the developed mathematical model for describing pulsatile blood flow in multiple-stenosed porous arteries. Consequently, the CFD analysis serves as an independent verification of the theoretical predictions and provides a detailed visualization of the underlying hemodynamic phenomena.

VII. Conclusions

This study investigates pulsatile blood flow through an axisymmetric porous artery with multiple stenoses and velocity slip at the permeable wall. Analytical and finite-volume numerical methods were employed to examine the effects of slip, magnetic field, and permeability on flow behavior. The results provide insights into velocity, wall shear stress, and the hemodynamic factors associated with vascular diseases such as atherosclerosis. Based on the computational findings, the following observations were made: A rise in slip parameter K_p correlated with reduced u_x, Q_v and τ_w in blood flow, due to weaker fluid-wall interaction.

- Increasing stenosis depth and magnetic parameter reduces velocity (u_x) and flow rate (Q_v), while increasing wall shear stress (τ_w).
- Higher permeability (λ) enhances flow, lowers pressure gradient, and reduces wall shear stress.
- Increasing Reynolds number (R) decreases velocity and flow rate but increases wall shear stress.
- CFD results showed flow acceleration at stenoses, pressure reduction along the artery, and peak wall shear stress near stenosis throats.
- Excellent agreement between analytical and CFD results validates the proposed model.

In summary, the present study combines analytical modeling and CFD simulations to investigate pulsatile blood flow through a porous artery containing multiple stenoses under slip boundary conditions. The obtained results demonstrate that stenosis severity, magnetic effects, permeability and Reynolds number significantly influence velocity distribution, volumetric flow rate, pressure characteristics, and wall shear stress. The excellent agreement between theoretical predictions and ANSYS Fluent simulations confirms the robustness of the proposed model. These findings may contribute to a better understanding of arterial flow behavior and provide useful guidance for the assessment and treatment of cardiovascular disorders associated with arterial narrowing.

References

[1] G. S. Beavers and D. D. Joseph, “Boundary conditions at a naturally permeable wall,” J. Fluid Mech., vol. 30, pp. 197–207, 1967.

[2] B. S. Bhatt, “On the analogy in slip flows—II,” Appl. Sci. Res., vol. 35, no. 1, pp. 37–41, Jan. 1979.

[3] X. Chen, Y. Zhan, Y. Fu, J. Lin, Y. Ji, C. Zhao, Y. Fang, and J. Wu, “The effect of stenosis rate and Reynolds number on local flow characteristics and plaque formation around the atherosclerotic stenosis,” Acta Bioeng. Biomech., vol. 23, no. 1, pp. 135–147, 2021.

[4] A. S. Dawood, F. A. Kroush, R. M. Abumandour and I. M. Eldesoky, “Comparative analysis of pulsatile nanofluid flow under slip conditions through stenosed arteries,” Boundary Value Probl., vol. 2025, Art. no. 28, 2025.

[5] I. M. Eldesoky, “Slip effects on the unsteady MHD pulsatile blood flow through porous medium in an artery under the effect of body acceleration,” Int. J. Math. Math. Sci., vol. 2012, Art. no. 860239, 2012.

[6] I. Eldesoky, “Unsteady MHD pulsatile blood flow through porous medium in stenotic channel with slip at permeable walls subjected to time dependent velocity (injection/suction),” Walailak J. Sci. Technol., vol. 11, pp. 901–922, Nov. 2014.

[7] J. Farooq and M. Hussain, “Analysis of MHD slip blood flow through a constricted artery filled with a porous medium of variable permeability: Applications in biomedical engineering,” Alexandria Eng. J., vol. 114, pp. 426–439, 2025.
[8] F. Shaikh, A. Shaikh, E. Hınçal, and S. Qureshi, “Comparative analysis of numerical simulations of blood flow through the segment of an artery in the presence of stenosis,” J. Appl. Math. Comput. Mech., vol. 22, pp. 49–61, Jun. 2023.
[9] S. Ganesh, V. W. J. Anand, P. Chandrasekar, and M. Anish, “Effects of magnetohydrodynamic unsteady fluid flow over a narrow channel in the axial and radial directions,” Int. J. Ambient Energy, vol. 43, no. 1, pp. 1368–1372, Dec. 2022.
[10] O. D. Makinde and T. Chinyoka, “Unsteady MHD flow in a porous channel with an exponentially decreasing suction,” J. Pure Appl. Math., vol. 1, no. 1, pp. 1–13, 2001.
[11] N. Satwai and K. M. Prasad, "Modelling of MHD micropolar nano fluid flow in an inclined porous stenosed artery with dilatation," East Eur. J. Phys., vol. 2025, no. 3, pp. 115–130, 2025.
[12] K. Thirunanasambantham, R. Sureshkumar, M. Venkatesan, and S. Rajan, “Computational analysis of hybrid GPL blood nanofluid flow through a stenosed artery under MHD effects,” Alexandria Eng. J., 2025.
[13] S. Mishra, S. U. Siddiqui, and A. Medhavi, “Blood flow through a composite stenosis in an artery with permeable wall,” Appl. Appl. Math. Int. J. (AAM), vol. 6, no. 1, 2011.
[14] O. D. Makinde and E. Osalusi, “MHD steady flow in a channel with slip at the permeable boundaries,” Rom. J. Phys., vol. 51, 2006.
[15] P. G. Saffman, “On the boundary condition at the surface of a porous medium,” Stud. Appl. Math., vol. 50, no. 2, pp. 93–101, Jun. 1971.
[16] J. C. Misra, A. Sinha, and G. C. Shit, “Mathematical modeling of blood flow in a porous vessel having double stenoses in the presence of an external magnetic field,” Int. J. Biomathematics, vol. 4, no. 2, pp. 207–225, Jun. 2011.
[17] G. C. Shit and M. Roy, Eds., “Hydromagnetic pulsating flow of blood in a constricted porous channel: A theoretical study,” in Proc. World Congress on Engineering, London, U.K., Jul. 4–6, 2012, vol. 1.
[18] A. Hussain, L. Sarwar, S. Akbar, and S. Nadeem, “Mathematical model for blood flow through the stenosed channel,” Phys. Scr., vol. 95, no. 2, Art. no. 025206, 2020.
[19] H. Girija Bai, “A numerical simulation of pressure variation in arteries affected by stenosis,” Res. J. Pharm. Technol., vol. 10, no. 3, pp. 802–810, 2017.
[20] H. Girija Bai, K. B. Naidu, and G. Vasanth Kumar, “Computational analysis of blood flow in abdominal aortic artery affected by acute stenosis,” J. Pure Appl. Microbiol., vol. 9, no. 3, pp. 2597–2610, 2015.
[21] M. Umar, F. Shahzad, A. Basit, N. U. Amin, and H. M. Ali, “Numerical simulations of blood flow in a stenosed artery using a multi-criteria decision-making algorithm,” Sci. Rep., vol. 16, p. 4527, 2026.